Proceedings World Geothermal Congress 2020+1
Reykjavik, Iceland, April - October 2021

Fault slip and fracture growth revealed by induced seismicity during a decameter-scale hydraulic stimulation experiment

Villiger, L.[1], Krietsch, H.[2], Gischig, V.S. [3], Doetsch, J. [2], Jalali, M.R. [4], Amann, F. [4], Wiemer, S.[1]

1. Swiss Seismological Service (SED), ETH Zürich, Sonneggstrasse 5, 8092 Zurich, Switzerland

2. Department of Earth Sciences, ETH Zurich, 8092 Zurich, Switzerland

3. CSD Ingenieure, 3097 Bern, Switzerland

4. Department of Engineering Geology & Hydrogeology, RWTH Aachen, Aachen, 52062, Germany

Correspondence to: linus.villiger@sed.ethz.ch

Keywords: Enhanced geothermal systems, seismo-hydro-mechanical processes, hydraulic stimulation mechanism, splay fracture, break in frequency magnitude scaling

ABSTRACT

Several high-pressure fluid injection experiments were performed on decameter scale at the Grimsel Test Site, Switzerland, in the framework of the In-Situ Stimulation and Circulation project. These experiments aimed for a better understanding of the link between induced seismicity and the underlying hydro-mechanically coupled processes associated with hydraulic stimulation. One of the performed experiments targeted one of two parallel, mature, brittle-ductile shear zones that dissect crystalline rock 5 m apart from each other, and bound a heavily fractured zone in between. The stimulation led to little change in injectivity as the initial injectivity was already high before the experiment. Nonetheless, the seismic response induced by 1.3 m^3 of injected fluid has been substantial with > 5000 detected events, more than 3000 of which could be located with an accuracy of < 0.5 m. Details of the seismicity clouds and observed deformation suggest ongoing stimulation of a fracture connecting the two neighboring shear zones. During a later stage of the experiment, a potential new fracture initiated from the target shear zone at a steep angle and propagated towards relatively unfractured rock. The fracture is interpreted as a splay fracture that is induced by stress transfer related to shear dislocation along the rough shear zone. Finally, the frequency magnitude distribution of the located seismic events show a break in scaling, and suggests a lower b-value for lower magnitude seismic events compared to a higher b-value for higher magnitude events. Together with the observations of pressure and deformation, the seismicity dataset provides insights on the hydraulic stimulation processes at an unprecedented level of detail.

1. INTRODUCTION

The enhanced geothermal system (EGS) concept foresees the advective heat extraction from hot rock masses by circulating a working fluid between injection and production wells. In central Europe, a sufficient rock mass temperature for an economic electric power production can be found at a depth of 4 – 6 km (Evans, 2014). However, the permeability of the rock at such depth – often crystalline rock - is usually too low to enable advective heat transport (Ingebritsen et al., 2010; Preisig et al., 2015). Thus, permeability has to be enhanced artificially by means of hydraulic stimulation, which usually involves high-rate or high-pressure fluid injections.

Yet, the EGS technology neither reached technical maturity nor economical standards (Jung, 2013), due to difficulty to hydraulically connect two or more boreholes and due to induced earthquakes that inevitably occur during stimulation. Projects, like the EGS project in Basel, Switzerland, or the one in Pohang, South Korea, have led to major set-backs because of the induced large magnitude earthquakes (Grigoli et al., 2018; Kang-Kun et al., 2019; Kim et al., 2018; Mignan et al., 2015). The need for improved control on the hydraulic stimulation process is indispensable for the EGS technology. The main goal is to create a sustainable heat exchanger at depth, and in the meantime, keep induced seismicity at an acceptable level, both during stimulation and operation.

The dominant end-member stimulation mechanism in EGS is found to be shearing of pre-existing fractures and faults (also known as hydraulic shearing, HS, i.e. mode-II, mode-III dislocation) (Fehler, 1989; Kelkar et al., 2016; Pine et al., 1984), which is evoked by fluid injection into pre-existing discontinuities (i.e., fractures and faults) supporting sub-critical level of shear stress. Shearing is induced by the pressure-related reduction in effective normal stresses across the discontinuities. The required fracture fluid pressure is lower than the minimal principal stress magnitude, but needs to be above shear strength of present discontinuities. Shear dislocation can lead to strong and irreversible enhancement of fracture permeability by 2-3 orders of magnitude, caused by the combination of shearing and dilation across a rough fracture plane with asperities. Thus, HS is often the preferred mechanism for permeability creation in the context of EGS. Another end-member stimulation mechanism involves creating and opening of new fractures by means of hydraulic fracturing (i.e., HF, mode-I), which ultimately connect to the pre-existing fracture network. Permeability enhancement by HF alone is mostly reversible, if no proppants are injected into the fracture/fault. It has been observed that both HS and HF mechanisms may occur simultaneously during hydraulic stimulations (Krietsch et al., in preparation; McClure et al., 2014b). Often the creation of new fractures is associated with stress transfer induced by shearing leading to mixed-mode fracture dislocations that may be interpreted as splay fractures (e.g., McClure et al., 2014a).

Although hydraulic shearing is associated with induced earthquakes, it has been shown that a large portion of shear dislocation is aseismic (Cappa et al., 2018; Guglielmi et al., 2015). Seismic energy is only radiated when slip velocities are rapid enough. The severity of a seismic response to fluid injection may also be linked to the present geological setting. McClure et al. (2014b) relates fault properties from wellbore observations of six field scale hydraulic stimulations in granitic rock to the severity of seismic response, and suspects a possible correlation between maturity of fault development (i.e., well-developed brittle fault zones) and seismic moment release.

To gain a better understanding of the hydro-mechanically coupled processes and the linked induced seismicity occurring during the stimulation process, we conducted 12 hydraulic stimulation experiments in a decameter-sized crystalline rock volume at the Grimsel Test Site (GTS) as part of the In-Situ Stimulation and Circulation (ISC) project (Amann et al., 2018). Six experiments targeted different pre-existing shear zones for reactivation, and six experiments initiated new hydraulic fractures. To capture the seismo-hydro-mechanical responses of the target rock mass and the target shear zones, a comprehensive monitoring system was installed along tunnel walls and within 10 boreholes. The results of all six conducted HS experiments within the ISC project will be published by Krietsch et al. (in preparation). Dutler et al. (2019) analyzed the six HF experiments. The overall seismic response during all 12 experiments will be published by (Villiger et al., in preparation).

In this contribution, we present a detailed analysis of the observations during one of the 12 injection experiments (i.e., HS4). Experiment HS4 targeted one of the highly fractured brittle-ductile shear zones (i.e., S3.1 sub-vertical EW oriented) and adjacent fractures. It stands out because it produced the largest number of seismic events (Villiger et al. (in preparation) among all experiments, although the injection volume is similar for all experiments. In fact, more than half of the total seismic events from all 12 experiments were induced during this experiment. However, unlike the other experiments, seismicity is limited to mostly patches and clusters within a small radius from the injection interval (note that we here use the term “cluster” for a distinct subgroup of seismic events within the seismicity cloud of the injection experiments). We here present a detailed analysis of the spatial and temporal evolution of the seismicity cloud in connection with the ambient stress conditions.

2. METHODS

2.1 Study Site

The ISC project was carried out at the Grimsel Test Site (GTS), Switzerland (Figure 1a), an underground research facility operated by Nagra (i.e., National Cooperative for the Disposal of Radioactive Waste). An overburden of ~ 480 m overlays the test volume, which is located in the south of the GTS and accessible from three tunnels. Various boreholes with a length up to 47 m were drilled into the test volume for the purpose of fluid injections (i.e., two boreholes referred to as INJ), pressure monitoring (i.e., three holes referred to PRP), deformation monitoring (i.e., 3 FBS boreholes), geophysical monitoring (4 holes referred to as GEO), and stress measurements (3 boreholes, referred to as SBH) (see Figure 2). The geological model of the test volume was based on the characterization of these boreholes and the surrounding tunnel walls. The crystalline host rock in the test volume is relatively intact (0-3 fractures per meter) and is intersected by: a) four sub-vertical shear zones with a ductile deformation history striking NE-SW (referred to as S1 shear zones), and b) two additional shear zones (referred to as S3 shear zones) with a brittle-ductile deformation history, which are oriented sub horizontal E-W (Krietsch et al., 2018a). The two brittle-ductile shear zones are associated with biotite-rich metabasic dykes of up to 1 m thickness. Between the two brittle-ductile shear zones S3.1 and S3.2 the rock mass is heavily fractured in the eastern half of the test volume (towards the AU tunnel, Figure 1). Injection experiment HS4 analyzed in detail in this manuscript targets brittle-ductile shear zone S3.1 through injection borehole INJ1 (see detail in Figure 1a).

Stress characterization revealed a tectonic stress state with measured 30 m south of shear zone S3.1 (dip direction/dip of 104°/39° (σ_1 = 13.1 MPa), 259°/48° (σ_2 = 9.2 MPa), 004°/13° (σ_3 = 8.7 MPa)). It is assumed that these measurements are not influenced by the shear zones and is thus referred to as unperturbed stress state. The stress field in the close proximity to shear zone S3.1 (Figure 1a) (dip direction/dip of 134°/14° (σ_1 = 13.1 MPa), 026°/50° (σ_2 = 8.2 MPa), 235°/36° (σ_3 = 6.5 MPa)) was inferred from borehole SBH4, and is evidently perturbed by the shear zone. Note that this borehole intersects the shear zone roughly 20 m above the injection boreholes. For both stress states, slip tendencies were determined for all mapped discontinuities (Figure 1c, d). Slip tendency magnitudes inferred from the perturbed stress state (which was measured in close to experiment HS4) are larger for a majority of fractures as well as for the S3.1 and S3.2 structures. More information on the characterization of the test volume can be found in Krietsch et al. (2018b).

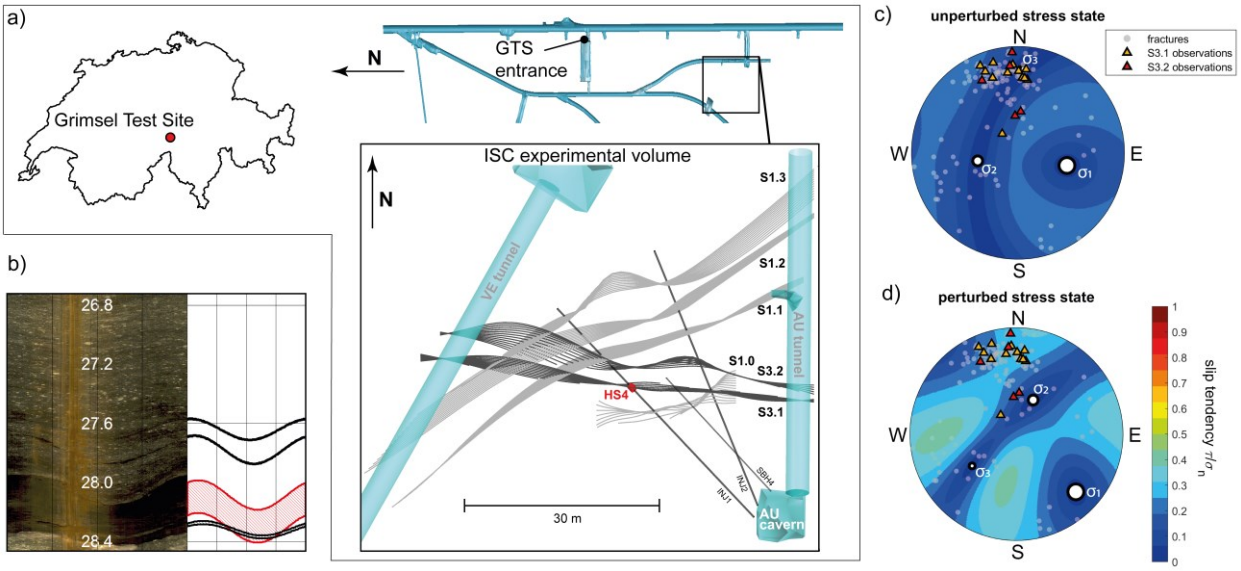

Figure 1: a) The location of the GTS in Switzerland (source: www.d-maps.com) in addition to the location of the ISC experimental volume within the GTS operated by NAGRA intersected by shear zones S1 and S3. In red color the HS4 injection interval of 1 m length. b) shows the optical televiewer recording of the injection interval of experiment HS4 (i.e., from 27.2 – 28.2 m) along with the observation of the metabasic dyke in red (i.e., the actual S3.1 shear zone) and adjacent fractures. c) shows principal stress directions of the unperturbed stress state and inferred slip tendencies.d) principal stress directions of the perturbed stress state with inferred slip tendencies, both with fracture and shear zone observations in boreholes (i.e., in INJ1, INJ2, FBS1, FBS2, FBS3, PRP1, PRP2, SBH4). (c) and d) are lower hemisphere stereographic projections)

2.2 Injection protocol

During the HS4 experiment, a total of ~1.3 m^3 of water was injected during four injection cycles (referred to as C1 – C4, Figure 3a), which were either pressure- or rate-controlled. All the cycles were followed by a shut-in and venting phase of 10 to 30 minutes duration (note: because of the "injected volume dependent" design of Figure 3a, shut-in and venting phases are not visible). The entire experiment lasted for about 6 hours and 30 minutes. The pressure-controlled cycles C1 and C2 were carried out to determine pre-stimulation jacking pressure and initial injectivity of the target structure. Cycle C3 is the main stimulation cycle. It was conducted rate-controlled and represents the cycle during which the bulk of fluid volume was injected. The goal of injection cycle C4 was to determine post jacking pressure and injectivity in a first pressure-controlled phase and a final flow-controlled phase.

2.3 Seismic monitoring and data processing

Seismicity was monitored by using 26 highly-sensitive piezo-electric acoustic emission sensors (termed piezosensors in this manuscript), from which eight were deployed in four monitoring boreholes (GEO1 – 4) at close proximity to the HS4 injection interval (i.e., within 16 m). For calibration purposes, five of the AE sensors were collocated by calibrating one component acceleromter. Seismic data was recorded continuously at a sampling rate of 200 kHz.

Seismic events were detected using a standard recursive STA/LTA coincidence trigger integrated in ObsPy, which is an open source Python library. Seismic event location was performed in a homogeneous, transversely isotropic velocity model. An amplitude based magnitude M_A was determined for located seismic events, correcting for angle dependent sensitivity variations and coupling quality of piezosensors. M_A were finally adjusted to absolute magnitudes M_W inferred for a subset of seismic events, which were recorded on accelerometers collocated with piezosensors on the tunnel wall (for more information on the seismic network, the detection, location and magnitude computation procedure we refer to Villiger et al. (in preparation)).

2.4 Monitoring pressure distribution and mechanical response

The hydraulic responses of the target shear zone were captured with 7 packed-off intervals installed along three boreholes (referred to PRP holes). Using a customized grout packer system, the monitoring intervals covered one or two shear zones that were the targets of the stimulations. The hydraulic pressures within the intervals were monitored at the uphole using Keller PAA33-X sensors with a resolution of 1 kPa. Here, we only present data from the monitoring intervals PRP1.2, PRP1.3 and PRP2.2 (Figure 2). Note that the interval names contain the borehole name plus and interval identification number, counted from borehole bottom to top.

A total of 60 fiber Bragg Grating (FBG) strain gages were used to capture the mechanical response of the target shear zones, adjacent fractures and the surrounding rock mass. The sensors, with a base length of 1 m were equally distributed over three boreholes (i.e., referred to FBS holes) that were fully grouted after sensor installation. The sensors measured deformations at a sampling rate of 1000 Hz with an accuracy of 1 με. Strain data were down sampled to 1 Hz by averaging 1000 samples, thus increasing the resolution to 0.1 με (Krietsch et al., 2018c). Here we only present selected FBG sensors that cover the target shear zone and adjacent fractures (Figure 2). The overall temporal and spatial evolution of the hydraulic and mechanical responses were analyzed by Krietsch et al. (in prep.). A more in depth description of the used monitoring systems and the experimental set up can be found in Doetsch et al. (2018)

3. RESULTS

3.1 Overall seismicity

In total, 3094 seismic events (out of 5607 detected events) in a magnitude range of M_A -5.5 to M_A -2.75 were successfully located. Of all located events, only 2.3% were recorded during venting and shut-in phases. The induced seismicity produced three distinct clusters (see Figure 2). The main cluster (Cluster 1, 2096 events of 3094 located events) propagates sub-vertically from the injection interval into direction ENE. It forms an acute angle to the target shear zone S3.1 (EW oriented) and consists of two main patches with high seismic event densities. Cluster 2 (784 events) formed higher up in the injection interval and propagates into EW direction, i.e. parallel to S3.1. It is divided into three patches that are smaller compared to the patches of Cluster 1. Also, a fourth patch with lower event density formed in Cluster 2 in upward direction. Cluster 3 (208 events) represents seismicity in a region where no pre-existing discontinuity was identified in the boreholes INJ and FBS2. The sparse seismicity of Cluster 4 (6 events) were induced in the S3.1-parallel S3.2 shear zone. Larger magnitude events (i.e., $M_A > -3.5$) are observed predominantly within the two patches of Cluster 1. Larger magnitude events are also observed at the southern periphery of Cluster 3. The large majority of seismic events were induced within a radius of 9 m from the injection interval, and surrounded by pressure and strain monitoring intervals (Figure 2).

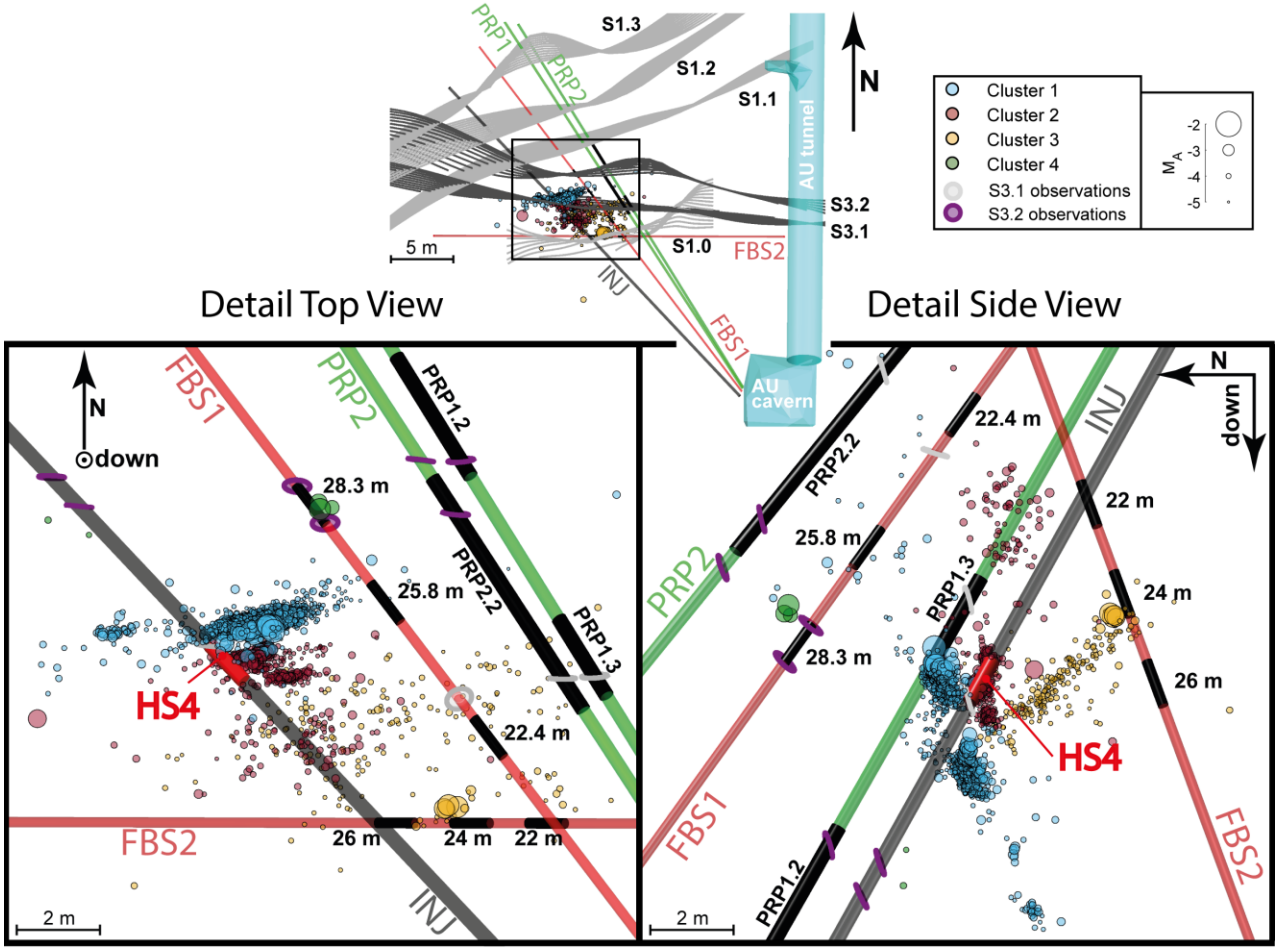

Figure 2: Overview in top a) and side view b) of the induced seismicity cloud and its clusters and patches during experiment HS4 as well as the measurement setup surrounding the injection. The injection borehole (black, INJ), the 1 m injection interval (red, HS4), as well as strain (red) and pressure (green) monitoring boreholes with measurement intervals (black). The target shear zone S3.1 observations in boreholes are indicated with grey discs and the parallel shear zone S3.2 is indicated by purple discs.

3.2 Temporal seismo-hydro-mechanical observations

To analyze the temporal evolution of seismicity, we present it along with injection parameters (i.e., injection rate, injection pressure), pressure observations, and strain data that are plotted against injected volume instead of time (Figure 3). During injection cycle C1, the onset of seismicity was at around 5.5 MPa injection pressure and 5 L/min flow rate. Seismic rates and magnitudes of Cluster 1 and 2 increase at the maximum injection pressure step of 7.8 MPa and 16.1 L/min. During cycle C1 one initial seismic event (green events/cluster) is induced in shear zone S3.2 parallel to the target shear zone S3.1. In cycle C2 the onset of seismicity occurs at an

injection pressure of 7.6 MPa and a flow rate of 8 L/min. At peak injection of injection cycle C2 (8 MPa, 14.8 L/min) seismicity is induced in Clusters 1, 2 and 4. Note that Cluster 2 is activated before Cluster 1 during Cycle C1, while the opposite is true during Cycle C2.

In the following cycle C3, during the first constant-rate step (10 L/min, 7 MPa) only sparse seismicity is observed. Seismicity rate picks up at the next rate-step (15 L/min), and a slightly increased injection pressure of around 7.6 MPa is observed. During the next constant flow rate steps (i.e., 20, 25 L/min), injection pressure is barely increasing and fluctuating in-between 7.4 and 7.6 MPa with the higher pressure levels occurring after the flow rate jumps. The decrease of injection pressure at constant rate steps is accompanied by a seismically quieter phase with decreasing event rate. The quiet phases occur at all three flow rate steps (C3.2, C.3.3 C3.4). Note that these rate decreases are not associated with short-lasting active seismic experiments conducted about every 10 minutes during the experiments (highlighted as grey shading in Figure 3). At the highest injection rate, Cluster 3 evolves with events in a dominant magnitude range of M_A – 5.5 to – 3.8, including four larger magnitude events (i.e., > M_A - 3.3). During cycle C4, only a single event is induced before maximum injection rate (i.e., 25L/min, ~8MPa). At this peak rate injection step, the pressure firstly increases but then decreases in a similar manner as during the constant flow-rate steps during injection cycle C3. During injection cycle C4, seismicity is predominantly induced in Cluster 1. Also the maximum magnitude event of this experiment (i.e., M_A = -2.75) occurs in this cycle.

Pressure monitoring intervals intersecting the target shear zone S3.1 (i.e, PRP1.3 and PRP2.2) indicated an almost linear increase of pressure with injected volume. A similar observation was made in the pressure monitoring interval intersecting shear zone S3.2 (i.e., PRP1.2). Note that the pressure signals in all three intervals were similar in magnitudes regardless of injection cycle and injection parameters (Figure 3b). In all the three intervals, the pressure at the start of each cycles is higher than at the beginning of the previous cycle, which indicates the limited pressure recovery. However, the rate of the pressure increase per injected volume remains constant over the four injection cycles.

The data of the longitudinal strain sensors acquired in borehole FBS1 presented in Figure 3c only shows the extensional strain. The borehole is intersecting to the shear zones S3.1 and S3.2 at a steep angle. The sensor at 22.4 m borehole depth lies south of the S3.1 target shear zone observation, the sensor at 25.8 m lies in-between the S3 shear zones within the heavily fractured zone, and the sensor at 28.3 m depth lies at the S3.2 shear zone. At the beginning of injection cycle C1, the sensor covering the target shear zone parallel to the S3.2 structure (at 28.3 m in FBS1) exhibits a higher strain rate compared to the sensors covering the target structure (22.4 m and 25.8 m in FBS1). A similar behavior can be observed during C2 and the first two injection steps of C3. With ongoing injection during C3, strain signals at all three presented sensors seem to plateau. With the following injection step, the target shear zone and the fractured zone again accommodate more extensional strain, while the target parallel to the shear zones stagnates at its strain level. At the end of injection cycle C3, strain magnitudes of the considered sensors reach their maximum with values below 100 με extensional strain (corresponds 1 micrometer given the 1 m sensor base length). The strain monitoring sensors in cycle C4 exhibit a sequence of extensions and contractions. Towards the maximum injected fluid, all the three intervals show a contractional (i.e., less extensional) character. However, compared to the pre-stimulation state, extensional residual strain is observed on all the tree intervals. The largest extensional residual strain was not observed across the target shear zone, but it was observed within the fractured zone between the two S3 shear zones.

In strain monitoring borehole FBS2, located south and parallel to the target shear zone S3.1, only marginal strain is observed until the half of the total volume has been injected halfway through cycle C3. Then, starting at an injected volume of 610 liters, the strain monitoring sensor at 22 m depth exhibits contraction as the injected fluid volume increases, whereby the sensor at 24 m depth experiences, after a short contraction phase, an extensive extensional phase to a magnitude of almost 400 με towards the end of cycle C3. Note that at the location of this sensor, no fracture was mapped before stimulation. The strain rate at this sensor accelerated when the injection flow rate was set to 25 L/min. This time step also marks the onset of seismic cluster 3. The sensor at 26 m borehole depth exhibits, after 610 liters injected fluid, an initial extensional phase, followed by a contractional phase, starting at the point in time where the highest extensional strain rate is observed at the sensor located at 24 m depth. During cycle C4, the strain monitoring intervals at 22 and 26 m exhibit contraction and, at later times, extension. This is opposite to the sensor in-between at 24 m depth, which experiences extension and stage contraction later. The residual strains measured 22 hours after the injection has started remain contractional at the sensor at 22 m depth, highly (i.e., ~120 με) and only slightly extensional at the sensors at 24 and 26 m depth, respectively.

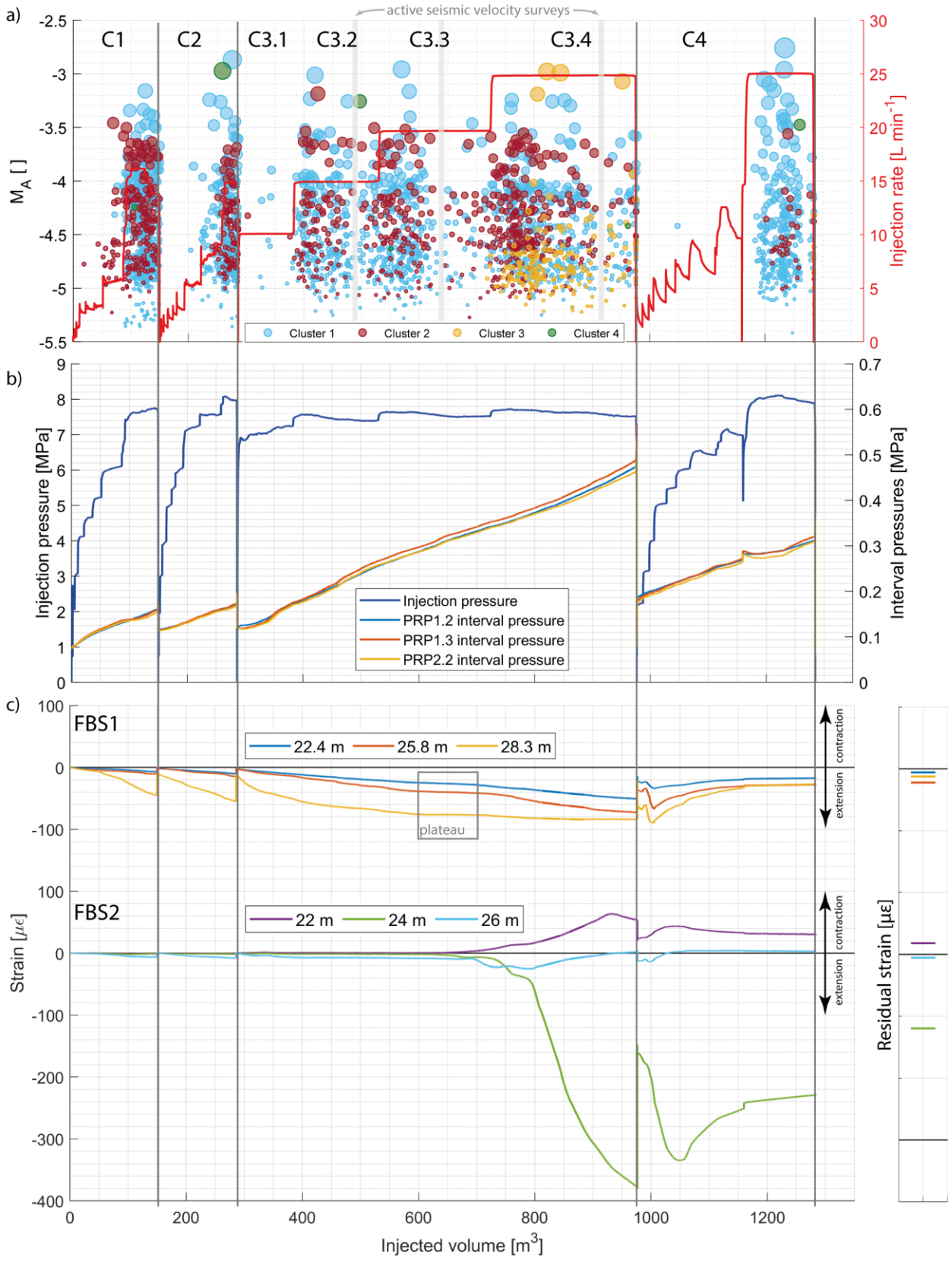

Figure 3: a) seismicity and injection rate of the four injection cycles (the shaded areas in cycle C3 indicate periods in time under which passive seismic event detection was on hold and active seismic surveys were performed), b) injection pressure and interval pressures, c) strain measurements of the different strain monitoring boreholes all dependent on injected fluid volume. The strain measurements are complimented with residual strain measured 22 hours after the injection has started.

3.3 Seismic event evolution

The temporal evolution of seismicity in Cluster 1 and 2 only shows a slight tendency of a propagating stimulation front (Figure 4, see blue events of lower patch of Cluster 1, which are accumulating at closer distance to the injection interval compared to later induced events). Seismic events are predominantly randomly distributed within the single patches. One exception represents Cluster 3, which is mainly induced during the final injection step (i.e., C3.4, Figure 3).

A closer look at Cluster 3 (Figure 4b) reveals that first seismic events are located close to the injection interval as well as in proximity to the lowest patch of Cluster 2. Over a time period of almost then minutes, Cluster 3 propagates from NW to SE. The six largest magnitude events of Cluster 3 are induced at close proximity to the strain monitoring interval at 24 m depth, which showed strong extensional strain during the occurrence of Cluster 3. It is noteworthy that extensional strain at the sensor 24 m already occurs at the very beginning of the seismicity Cluster 3, when seismicity clouds seems not to have propagated to the strain sensor yet (i.e. about 4 minutes after onset of Cluster 3).

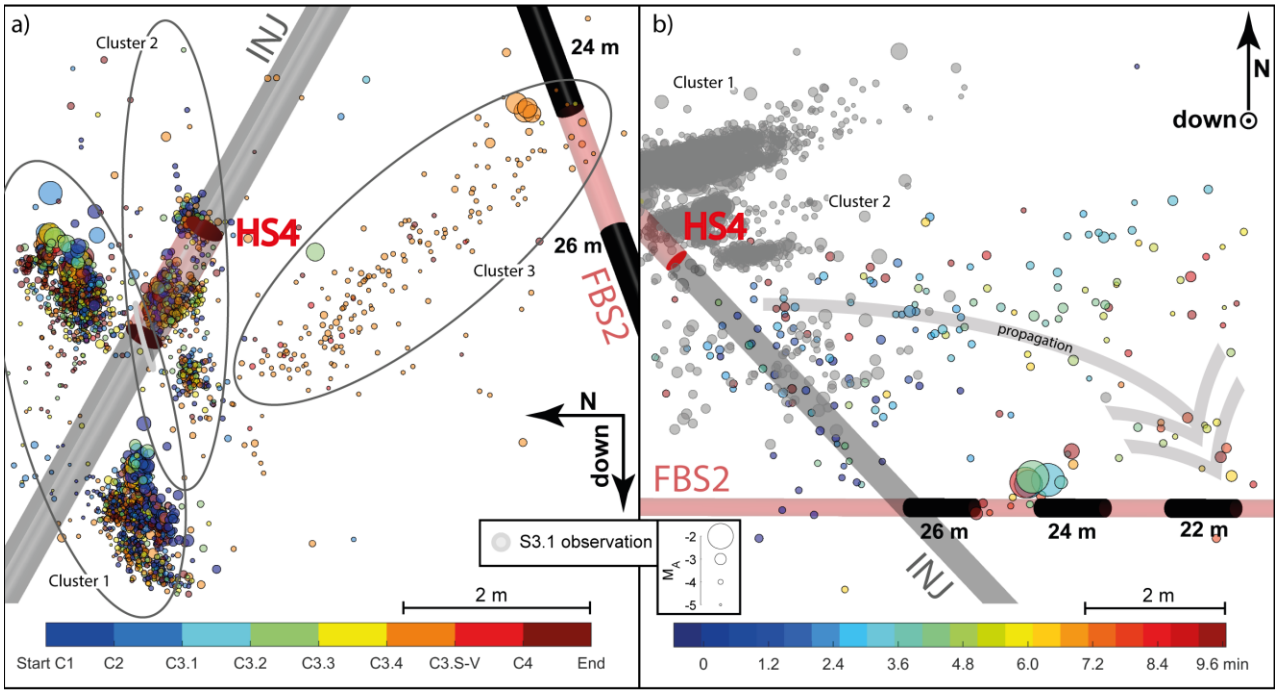

Figure 4: a) detailed side view of seismic event evolution of Cluster 1 – 3. The color coding represents the different cycles of the experiment, whereby cycle 3 exhibits a color change at every step rate increase (i.e., C3.1 – C3.4), also the shut-in and venting phase of cycle 3 (i.e., C3.S-V) is represented by a separate color. b) top view of event evolution of cluster 3, whereby the timing is referenced to the last step rate increase of cycle 3 (i.e., C3.4), the time where Cluster 3 was started to be formed.

3.4 Bimodal frequency magnitude distribution

The frequency magnitude distribution (FMD) of all recorded seismic events of experiment HS4 shows a break in scaling at M_A – 4.24 (Figure 5a, black line). The higher magnitude events above M_A – 4.24 scale with a b-value of 1.4 (Villiger et al., in preparation), whereby the lower magnitude events, below a magnitude of M_A – 4.24 scale at a lower b-value. Resolving the FMDs of three main clusters individually reveals that for Cluster 1, the bimodal characteristic remains. The FMD of Cluster 2 reveals an absence of higher magnitude (i.e., $M_A > -3.5$) events. The FMD of Cluster 3 shows a power law distribution below a magnitude of M_A – 4.24. However, the six higher magnitude events do not follow the same distribution.

The spatial distribution of seismic events above and below the break in scaling at M_A – 4.24 is shown in Figure 5b colored in red and blue, respectively. It can be observed that the events above the scaling break form sub clusters in proximity to the injection interval. However, for these 655 larger magnitude events, a higher b-value can be estimated compared to the 2439 lower magnitude events. The larger magnitude events responsible for the discrepancy from power law of Cluster 3 are located in close proximity to strain monitoring borehole FBS2 and the sensor at 24 m depth.

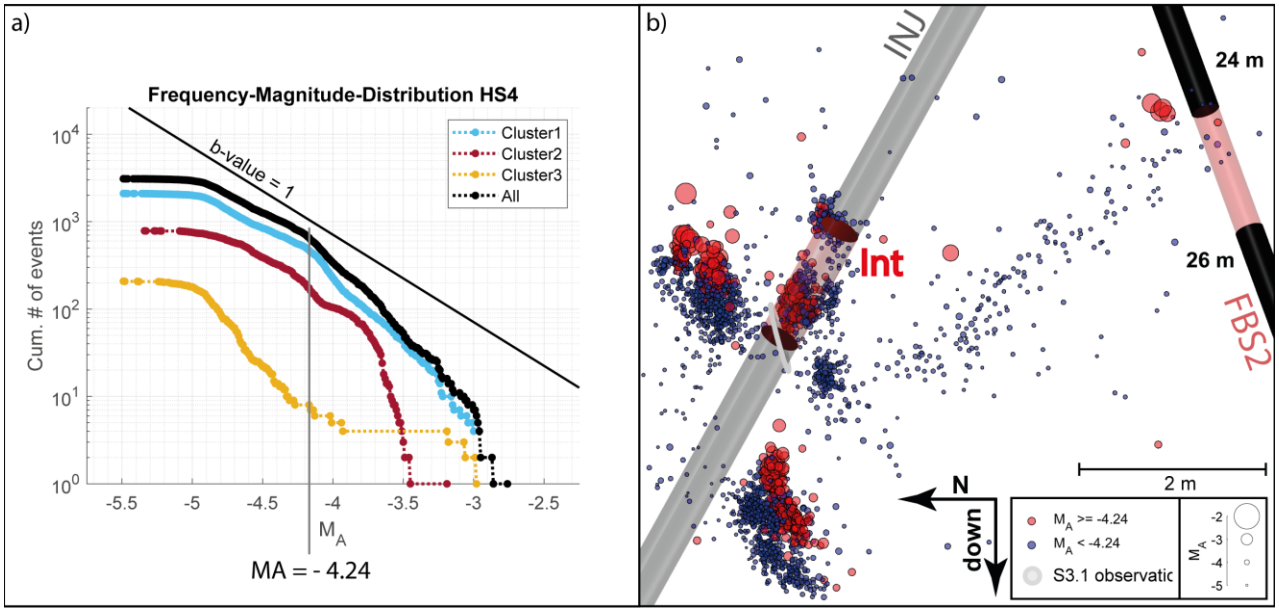

Figure 5: a) shows the FMD of experiment HS4 (black dotted line) adapted from Villiger et al. (in preparation) an its bimodal characteristic with the break in scaling at a magnitude of -4.24. Furthermore, the FMDs of the individual clusters are shown (colored dotted lines). b) shows a side view of the main seismicity clusters introduced in Figure 2 in detail. Here, the seismic events below the scaling break at a magnitude of -4.24 are colored in blue, seismic events above are colored in red.

4. DISCUSSION AND CONCLUSION

4.1 Injected-volume-dependent deformation

From the start of injection, this heavily fractured rock volume is highly transmissive, as the pressure intervals intersecting the target shear zone (S3.1, PRP1.3), the parallel shear zone (S3.2, PRP1.2) or both (PRP2.2) show almost identical, immediate, and linear pressure increase with injected volume. Furthermore, pressure in the monitoring intervals indicate no steep pressure increases to magnitudes as high as the injection pressure, which would be an indication for pressure fronts (non-linear pressure diffusion) related to a strong permeability increase around these intervals. Instead, the monitoring locations exhibit a behavior that is possibly explained with a linear pressure diffusion. Also strain observations in the first half of the experiment suggest that the fastest and strongest mechanical response occurs in the shear zone S3.2 structure that is parallel to the target. The strongest permanent deformation was found in the fractured zone in-between the two S3 shear zones.

Seismically, Cluster 1 suggests an ongoing stimulation of a structure that is oblique to the target shear zone S3.1 and connects the injection interval to the shear zone S3.2 (Figure 6a). The cluster contains most of the seismic events. Additionally, the strain sensor in between the two S3 shear zones experienced the largest permanent deformation compared to the other two presented sensors in FBS1. This may indicate a strong seismically active shear dislocation within the fractured zone next to the target shear zone. This stimulated connection explains the hydraulic connection between shear zone S3.1 and S3.2. Cluster 2, oriented parallel to the target shear zone S3.1 suggests the stimulation of fractures parallel to the target shear zone or the intersection between the heavily fractured host rock and the metabasic dyke of the target shear zone.

We interpret Cluster 1 and 2 to represent ongoing hydraulic shearing of S3.1 and the surrounding fractures (i.e., mode-II, mode-III deformation) during the first half of the total injected fluid volume. As a secondary mechanically-induced process, starting at 610 liters of injected fluid, a potentially new fracture starts to form with initially no observed seismicity. At the step rate increase to 25 L/min of injected fluid the opening of the initiated fracture starts to accelerate (Figure 3, FBS2, monitoring interval at 24 m) and seismicity of Cluster 3 begins. The initiated opening mode fracture then propagates over a duration of ten minutes in direction SE (Figure 4b). The magnitude of residual strain (120 micrometer, Figure 3c) suggests that aside of opening mode deformation, this newly initiated fracture also produced shear mode deformation. The current hypothesis is that this fracture is a so-called splay fracture (Jung, 2013; Krietsch et al., in preparation; McClure et al., 2014a; Villiger et al., in preparation). Such secondary fractures form due to shearing induced stress transfer around the dislocated area of a rough fracture surface. Because of the orientation of this initially tensile fracture (normal to sigma 3 of the perturbed stress state), seismicity is only induced once fluid enters the fracture pressurizes it and induced shear failure around the opening fracture through pressure leak-off. The strong extension at the strain sensor at 24 m in FBS2 is compensated by contraction of the neighboring strain sensors (i.e.at 22 and 26 m).

Shear dislocation along the target shear zone is only possible assuming stress condition corresponding to the perturbed in-situ stress field (Krietsch et al., 2018b) (Figure 1d). The overall induced shearing along the target shear zone is characterized as a dextral strike-slip faulting (Figure 6b). Note that the shape of the newly formed fracture – interpreted as splay fracture – contradicts the expected propagation direction for a splay fracture given observed shear sense along the S3.1 shear zone. Although we acknowledge that other interpretations of newly formed structures may be valid, we indicate that the shearing induced stress redistribution induced the splay fracture which rotated with ongoing propagation into an orientation favorable for the in-situ stress state. Thus, it has a mode-I character, which is consistent with the large reversible strain component observed in the FBS2 borehole.

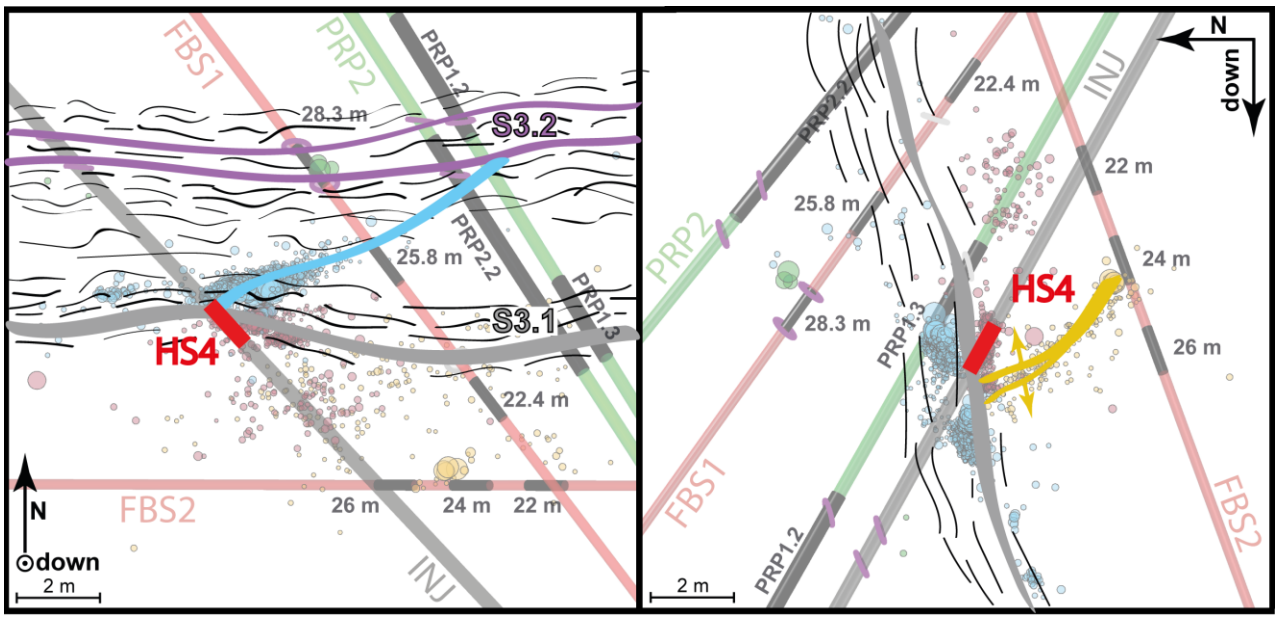

Figure 6: a) top view of conceptual interpretation of the diagonal hydraulic connection (blue) between the S3.1 target shear zone and the parallel S3.2 shear zone. b) side view of conceptual interpretation of the initiation of a splay fracture (yellow).

4.2 The bimodal frequency magnitude distribution

When reasoning for the break in scaling of the recorded seismic events during experiment HS4, one cannot avoid suspecting that seismic events were also missed above the implied completeness level (i.e., for experiment HS4 at M_A -4.9). One reason for undetected events in the full range from small to large magnitudes is that event detection was on hold during active seismic velocity measurements (i.e., active seismic surveys, Figure 3) performed throughout the experiment (Doetsch et al., 2018). Another reason for undetected seismic events in the full magnitude range might be the saturation of the detection algorithm during high seismic event rates. However, we argue that these effects would compromise the entire magnitude range in a similar way and therefore do not explain a bimodal frequency magnitude distribution.

The low b-value below M_A-4.24 may be interpreted as missing a large number of small magnitude seismic events. One reason for missing out small magnitude events may be a heterogeneous network sensitivity within the volume of interest. This experiment was performed in the focus point of the seismic network, and the extent of the majority of the seismic events are within a radius of 9 m of the injection interval with most seismicity located in clusters around 4 m from injection. Thus, we argue that the network sensitivity is sufficiently constant within the volume. Furthermore, during injection experiment HS5, which was performed only 3 m apart from experiment HS4, an M_C of – 4.8 was observed and the FMD shows no bimodal characteristic (Villiger et al., in preparation).

We thus argue that the bimodal FMD characteristic is not a detection artifact but may have underlying physical reason. The fact that we observe a strong clustering, in particular also of the larger magnitude events, may suggest that the size of preexisting fractures strongly defines the size distribution of earthquakes. Thus, the bimodal distribution of earthquakes may reflect a bimodal distribution of fracture sizes. The clustering of larger magnitude events closer to the injection interval may also be associated to an increased pressure perturbation compared to seismic events further away from the injection interval.

Also drilling induced stress changes in proximity of the borehole may result in a heterogeneous seismic event distribution. This hypothesis is supported by Cluster 3, which is associated with the newly initiated splay fracture. The large magnitude events in Cluster 3 are located close to the borehole FBS2 may be related to local stress perturbations or changing material properties due to the grouted infill of the borehole.

5. CONCLUSION AND OUTLOOK

For this contribution, we analyzed one of 12 hydraulic stimulation experiments performed in a crystalline rock volume of about 20 x 20 x 20 m size in detail. The experiment differs from the 12 other experiments in that 1) the highest pre-injectivity was measured, 2) the injectivity was not increased during the stimulation treatment, and 3) the seismic response was by far most intense. The stimulation targeted one of two parallel brittle-ductile shear zones which are associated with biotite-rich metabasic dykes. In-between the shear zones, the rock mass is observed to be heavily fractured.

Detailed insights into the seismo-hydro-mechanical response of a target shear zone and the adjacent fracture network were gained from high resolution monitoring. Permanent deformations show that the stimulation was more effective within the fracture network next to the actual target shear zone, compared to the initially highly transmissive target shear zone. Additionally, the formation and propagation of a splay fracture was observed from seismicity and deformation data.

We further discuss reasons for the break in scaling observed in the frequency magnitude distribution of the seismic events induced during stimulation experiment HS4. Possibly, a fracture size distribution following a composite of two or more distinct fractal distributions may be the underlying reason for a bimodal frequency magnitude distribution.

Dislocation along the deformation around the target shear zone S3.1 has led to a new fracture propagating off the S3.1 shear zone - a structure currently interpreted as a splay fracture. Better understanding of these processes may be gained from moment tensor inversion of the seismic events which exhibit an adequate number of arrivals in good spatial coverage. Moment tensor inversion using the software HybridMT (Kwiatek et al., 2016) is the scope of future work.

For a more complete catalog and more reliable magnitude estimates, we intend to use the matched filter technique and the relative magnitude computation approach introduced by Herrmann et al. (2019). To investigate the influence of the spatial distribution of the magnitude of completeness, we intend to perform a spatial probability-based completeness study in 3D (Schorlemmer et al., 2008).

ACKNOLEDGMENTS

This study is part of the In-situ Stimulation and Circulation (ISC) project established by the Swiss Competence Center for Energy Research - Supply of Electricity (SCCER-SoE) with the support of the Innosuisse. Funding for the ISC project was provided by the ETH Foundation with grants from Shell and EWZ and by the Swiss Federal Office of Energy through a P&D grant. Linus Villiger is supported by the grant ETH-35 16-1. Hannes Krietsch is supported by the SNF grant 200021_169178. The Grimsel Test Site is operated by Nagra, the National Cooperative for the Disposal of Radioactive Waste. We are indebted to Nagra for hosting the ISC experiment in their GTS facility and to the Nagra technical staff for onsite support.

REFERENCES

Amann, F., Gischig, V., Evans, K., Doetsch, J., Jalali, R., Valley, B., . . . Brixel, B. (2018). The seismo-hydromechanical behavior during deep geothermal reservoir stimulations: open questions tackled in a decameter-scale in situ stimulation experiment. *Solid Earth, 9*(1), 115-137.

Cappa, F., Guglielmi, Y., Nussbaum, C., & Birkholzer, J. (2018). On the relationship between fault permeability increases, induced stress perturbation and the growth of aseismic slip during fluid injection. *Geophysical Research Letters*.

Doetsch, J., Gischig, V., Villiger, L., Krietsch, H., Nejati, M., Amann, F., . . . Wiemer, S. (2018). Subsurface Fluid Pressure and Rock Deformation Monitoring using Seismic Velocity Observations. *Geophysical Research Letters*.

Dutler, N., Valley, B., Gischig, V., Villiger, L., Krietsch, H., Doetsch, J., . . . Amann, F. (2019). Hydraulic fracture propagation in heterogenous stress field in crystalline rock mass. *Solid Earth Discussion paper*.

Evans. (2014). *Reservoir Creation, in Energy from the Earth - Deep Gethermal as a Resource for the Future?* (S. Hirschberg, S. Wiemer, & P. Burgherr Eds. Vol. 62): vdf Hochschulverlag AG.

Fehler, M. C. (1989). *Stress control of seismicity patterns observed during hydraulic fracturing experiments at the Fenton Hill hot dry rock geothermal energy site, New Mexico.* Paper presented at the International Journal of Rock Mechanics and Mining Sciences & Geomechanics Abstracts.

Grigoli, F., Cesca, S., Rinaldi, A., Manconi, A., López-Comino, J., Clinton, J., . . . Wiemer, S. (2018). The November 2017 Mw 5.5 Pohang earthquake: A possible case of induced seismicity in South Korea. *Science, 360*(6392), 1003-1006.

Guglielmi, Y., Cappa, F., Avouac, J.-P., Henry, P., & Elsworth, D. (2015). Seismicity triggered by fluid injection–induced aseismic slip. *Science, 348*(6240), 1224-1226.

Ingebritsen, S. E., & Manning, C. (2010). Permeability of the continental crust: Dynamic variations inferred from seismicity and metamorphism. *Geofluids, 10*(1 2), 193-205.

Jung, R. (2013). *EGS - goodbye or back to the future.* Paper presented at the ISRM International Conference for Effective and Sustainable Hydraulic Fracturing.

Kang-Kun, L., Korea, G. S. o., (KERT), K. E. R. T., Eaertquake, K. G. C. o. t. C. o. t. P., & (ORAC), O. R. A. C. (2019). Summary Report of the Korean Government Commission on Relations between the 2017 Pohang Earquake and EGS Projekt.

Kelkar, S., WoldeGabriel, G., & Rehfeldt, K. (2016). Lessons learned from the pioneering hot dry rock project at Fenton Hill, USA. *Geothermics, 63*, 5-14.

Kim, K.-H., Ree, J.-H., Kim, Y., Kim, S., Kang, S. Y., & Seo, W. (2018). Assessing whether the 2017 Mw 5.4 Pohang earthquake in South Korea was an induced event. *Science*, eaat6081.

Krietsch, H., Doetsch, J., Dutler, N., Jalali, M., Gischig, V., Loew, S., & Amann, F. (2018a). Comprehensive geological dataset describing a crystalline rock mass for hydraulic stimulation experiments. *Scientific data, 5*, 180269.

Krietsch, H., Gischig, V., Doetsch, J., Evansm, K. F., Villiger, L., Jalali, M. R., . . . Amann, F. (in preparation). Hydro-mechanical processes and their influence on the stimulated volume: Observations from a decameter-scale hydraulic stimulation experiment.

Krietsch, H., Gischig, V., Evans, K., Doetsch, J., Dutler, N. O., Valley, B., & Amann, F. (2018b). Stress Measurements for an In Situ Stimulation Experiment in Crystalline Rock: Integration of Induced Seismicity, Stress Relief and Hydraulic Methods. *Rock Mechanics and Rock Engineering*, 1-26.

Krietsch, H., Gischig, V., Jalali, M., Doetsch, J., Valley, B., & Amann, F. (2018c). *A comparison of FBG-and Brillouin-strain sensing in the framework of a decameter-scale hydraulic stimulation experiment.* Paper presented at the 52nd US Rock Mechanics/Geomechanics Symposium.

Kwiatek, G., Martínez-Garzón, P., & Bohnhoff, M. (2016). HybridMT: A MATLAB/shell environment package for seismic moment tensor inversion and refinement. *Seismological Research Letters, 87*(4), 964-976.

McClure, M., & Horne, R. (2014a). An investigation of stimulation mechanisms in Enhanced Geothermal Systems. *International Journal of Rock Mechanics and Mining Sciences, 72*, 242-260.

McClure, M. W., & Horne, R. N. (2014b). Correlations between formation properties and induced seismicity during high pressure injection into granitic rock. *Engineering Geology, 175*, 74-80.

Mignan, A., Landtwing, D., Kästli, P., Mena, B., & Wiemer, S. (2015). Induced seismicity risk analysis of the 2006 Basel, Switzerland, Enhanced Geothermal System project: Influence of uncertainties on risk mitigation. *Geothermics, 53*, 133-146.

Pine, R., & Batchelor, A. (1984). *Downward migration of shearing in jointed rock during hydraulic injections.* Paper presented at the International Journal of Rock Mechanics and Mining Sciences & Geomechanics Abstracts.

Preisig, G., Eberhardt, E., Gischig, V. S., Roche, V., Van der Baan, M., Valley, B., . . . Lowther, R. (2015). Development of connected permeability in massive crystalline rocks through hydraulic fracture propagation and shearing accompanying fluid injection. *Geofluids, 15*(1-2), 321-337.

Schorlemmer, D., & Woessner, J. (2008). Probability of detecting an earthquake. *Bulletin of the Seismological Society of America, 98*(5), 2103-2117.

Villiger, L., Gischig, V., Doetsch, J., Krietsch, H., Dutler, N., Jalali, M. R., . . . Giardini, D. (in preparation). Influence of reservoir geology on seismic response during decameter scale hydraulic stimulations in crystalline rock.